ORIGINAL ARTICLE

Journal of Otorhinolaryngology and Facial Plastic Surgery 2023;9(1):1-9.

https://doi.org/10.22037/orlfps.v9i1.46872

Morphometric Analysis of Sphenopalatine Foramen on Computed Tomography Imaging for localization of Sphenopalatine Artery

Afsoon Zandi[1], Ali Safavi Naini[2,3*], Jahangir Ghorbani[1,3], Nasim Raad[1,3], Mahboobeh Karimi-Galougahi[1,4]

1 .Department of Otorhinolaryngology, Masih Daneshvari Hospital, Shahid Beheshti University of Medical Sciences, Tehran, Iran.

2. Hearing Disorders Research Center, Loghman Hakim Hospital, Shahid Beheshti University of Medical Sciences, Tehran, Iran.

3. National Research Institute of Tuberculosis and Lung Diseases, Masih Daneshvari Hospital, Shahid Beheshti University of Medical Sciences, Tehran, Iran.

4. Department of Otorhinolaryngology, School of Medicine, Chronic Respiratory Diseases Research Center, National Research Institute of Tuberculosis and Lung Diseases, Dr. Masih Daneshvari Hospital, Shahid Beheshti University of Medical Sciences, Iran, Tehran.

Article Info

Article Note:
Received: November 2023
Accepted: November 2023
Publish Online: December 2023

***Corresponding Author:**
Dr. Ali Safavi Naini
Email:
seydalisafavinaini@gmail.com

Keywords:
Sphenopalatine;
Foramen;
Epistaxis;
Endoscopic sinus surgery;
Computed tomography.

Abstract

Background: Epistaxis affects about 10% of those seeking medical treatment, with posterior epistaxis from the sphenopalatine artery (SPA) posing management challenges. The sphenopalatine foramen (SPF) is crucial for interventions, and CT imaging aids preoperative planning by detailing the SPF and adjacent structures.
Aim: Performing a morphometric analysis of the sphenopalatine foramen using CT imaging to identify and quantify anatomical landmarks that help surgeons locate the sphenopalatine artery.

Methods: A retrospective observational study analyzed Sinus CT scans from 200 adult patients to measure the sphenopalatine foramen's anteroposterior and craniocaudal dimensions. Distances from the SPF to key anatomical landmarks, such as the maxillary line and anterior head of the middle turbinate, were also measured. Statistical analysis was performed to assess variations based on sex and side of the nasal cavity, with a significance level set at $p < 0.05$.

Results: The average size of the SPF was 5.01 mm ± 1.37 in the anteroposterior dimension and 5.58 mm ± 1.71 in the craniocaudal dimension. The mean distances to anatomical landmarks were as follows: maxillary line 35.73 mm ± 2.47, anterior head of the middle turbinate 33.76 mm ± 4.52, basal lamella 9.71 mm ± 1.84, choanal arch 8.78 mm ± 1.62, posterior fontanelle of the maxillary sinus ostium 14.49 mm ± 1.32, and the bony attachment of the inferior turbinate 13.89 mm ± 2.01. The height above the nasal floor was 25.69 mm ± 2.43. Males exhibited longer distances to key landmarks compared to females, with no significant differences noted between the right and left nasal cavity sides.
Conclusion: Preoperative CT imaging effectively identifies key bony landmarks for accurately locating the sphenopalatine foramen, enhancing the safety and efficiency of endoscopic approaches to the sphenopalatine artery, especially in managing posterior epistaxis.

Conflicts of Interest: The Authors declare no conflicts of interest.
Please cite this article as: Zandi A, Safavi Naini Ali, Ghorbani J, Raad N, Karimi-Galougahi M. Morphometric Analysis of Sphenopalatine Foramen on Computed Tomography Imaging for localization of Sphenopalatine Artery. J Otorhinolaryngol Facial Plast Surg 2023;9(1):1-9. https://doi.org/10.22037/orlfps.v9i1.46872

Introduction

Epistaxis is a prevalent condition, impacting up to 60% of the global population at some point in their lives. Although many cases are mild and self-limiting, around 10% of individuals with epistaxis require medical intervention, highlighting its significance as a frequent

Journal of Otorhinolaryngology and Facial Plastic Surgery 2023;9(1):1-9.
https://doi.org/10.22037/orlfps.v9i1.46872

otolaryngology emergency (1). Epistaxis is typically divided into anterior and posterior types, based on the anatomical site of the bleeding. Anterior epistaxis is most often associated with Little's area, where the Kiesselbach plexus, a network of blood vessels, is located. This region is particularly vulnerable to trauma and environmental factors, making it the most common site of anterior nosebleeds. Comparatively, posterior epistaxis originates from Woodruff's area, which is supplied by branches of the sphenopalatine artery (SPA) (2,3). The SPA plays a critical role in providing blood to the lateral nasal wall and parts of the nasal cavity, making it the predominant source of posterior nosebleeds, which are often more severe and challenging to manage (3,4).

Effective management of epistaxis involves rapid identification and control of the bleeding site. Initial treatment strategies typically include non-invasive methods such as nasal packing, which is designed to apply pressure to the bleeding vessels. However, when these measures fail, more invasive interventions may be necessary. These can include arterial ligation, where the bleeding artery is surgically tied off, or endoscopic procedures that target the source of the hemorrhage directly. For severe or recurrent cases of posterior epistaxis, SPA ligation has emerged as a highly effective treatment option, with reported success rates ranging from 87% to 100% (5). This high efficacy underscores the importance of precise anatomical knowledge and surgical skill in managing this condition.

The sphenopalatine foramen (SPF) is a key anatomical landmark in endoscopic sinus surgery, serving as the entry point for the SPA into the nasal cavity and as a potential site for various nasal pathologies, including tumors and inflammatory conditions. The complexity of the SPF's anatomy, combined with variations in its surrounding structures, can pose significant challenges during surgery. In particular, these anatomical variations can hinder intraoperative visualization, making it difficult for surgeons to accurately identify and navigate the SPF, which may lead to complications or incomplete treatment (6).

Given these challenges, there is a clear need for a detailed understanding of the SPF’s anatomical features and its spatial relationship with other fixed landmarks within the nasal cavity. This study seeks to fill this gap by conducting a comprehensive morphometric analysis of the SPF using computed tomography (CT) imaging. By establishing reliable anatomical landmarks, the findings of this research aim to enhance the accuracy of SPA localization during surgical procedures, thereby improving the safety and efficacy of endoscopic sinus surgeries. Additionally, the study provides surgeons with critical information that can aid in preoperative planning, enabling them to anticipate and address potential anatomical challenges, ultimately leading to better surgical outcomes and reduced complication rates.

Methods

This research was conducted in accordance with the ethical principles outlined by the Declaration of Helsinki for studies involving human participants. A total of 200 patients, all of whom were at least eighteen years old, were included in the study.

These patients underwent sinus CT scans at Masih Daneshvari Hospital, and their imaging data were analyzed. The CT scans adhered to specific technical parameters: the scans were taken with the patients lying in a supine position, and the X-ray beam was aligned parallel to the hard palate. The images were captured with a slice thickness of 0.625 mm and a slice spacing of 0.4 mm. The scanning protocol included settings of 110 kV, with a bone window configured at W: 2000 and L: 400, and a soft tissue window at W: 140 and L: 40. Patients who had undergone previous surgery or experienced trauma that resulted in alterations to the paranasal sinuses or skull base, as well as those with congenital cranial

Journal of Otorhinolaryngology and Facial Plastic Surgery 2023;9(1):1-9.
https://doi.org/10.22037/orlfps.v9i1.46872

deformities or significant sinonasal obstructions, were excluded from the study.

The CT images were obtained using a 16-slice CT scanner (SOMATOM Scope, Siemens, Germany). The images were processed and analyzed using INFINITT PACS software, which facilitated the reading, rendering, and examination of the sphenopalatine foramen (SPF) in the CT images. The data were carefully reviewed to ensure adherence to established standards, ensuring that no critical details were overlooked.

Measurements were conducted on both axial and coronal planes. In the axial plane, the anteroposterior dimensions of the SPF were measured, as well as the distances from the SPF to various anatomical landmarks, including the maxillary line, the anterior head of the middle turbinate, the basal lamella of the middle turbinate, the choanal arch, and the posterior fontanelle of the maxillary sinus ostium (as illustrated in Figure 1). On the coronal plane, the craniocaudal dimensions of the SPF were measured, along with the vertical distances from the SPF floor to the nasal floor and the bony attachment of the inferior turbinate (as depicted in Figure 2). The collected measurements were then analyzed using SPSS software version 20.0 (IBM Corp., Armonk, NY, USA).

Qualitative data were presented as frequencies and percentages, and comparisons between groups were made using Fisher's Exact test. For quantitative data, which were normally distributed, results were expressed as mean ± standard deviation, and comparisons between sexes and sides of the nose were conducted using the student's t-test. A p-value of less than 0.05 was considered as statistically significant.

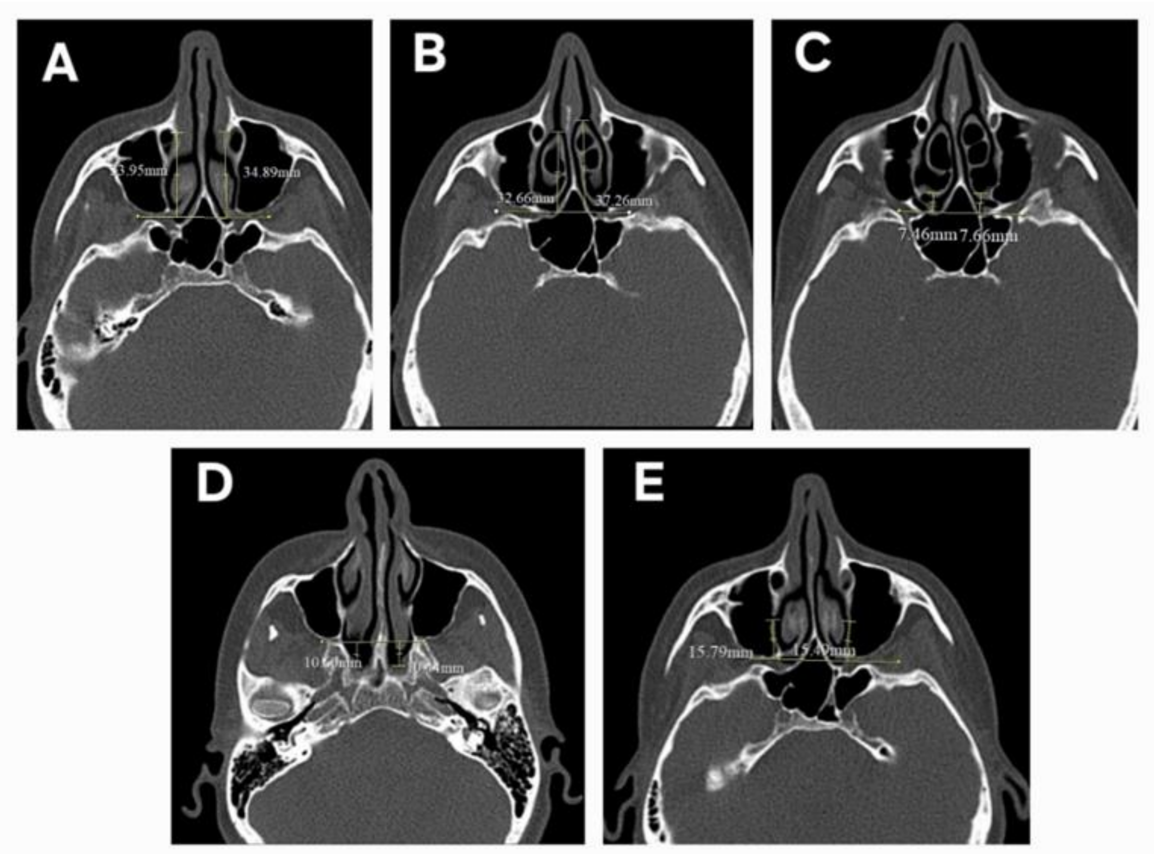

Figure 1. Computed tomography measurements for distances between sphenopalatine foramen and maxillary line (A), anterior head of the middle turbinate (B), basal lamella (C), choanal arch (D), posterior fontanel (E).

Journal of Otorhinolaryngology and Facial Plastic Surgery 2023;9(1):1-9.
https://doi.org/10.22037/orlfps.v9i1.46872

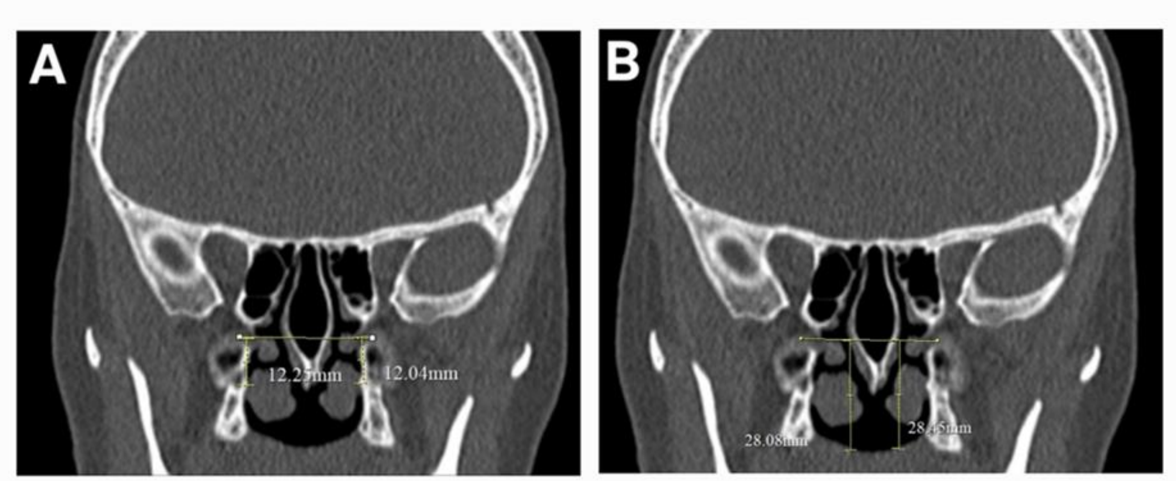

Figure 2. Computed tomography measurements for distances between sphenopalatine foramen and maxillary line (A), bony attachment of the inferior turbinate (B).

Results

The study included a total of 200 adult participants, yielding measurements for 400 sphenopalatine foramina (SPFs) and resulting in 3600 individual data points. The cohort consisted of 60% males (n=120) and 40% females (n=80), with an average age of 42.8 years ± 9.28, spanning from 20 to 65 years of age**.** In terms of the anteroposterior dimension, the average size of the SPF was 5.01 mm ± 1.37. The craniocaudal dimension averaged slightly larger at 5.58 mm ± 1.71. The mean distance from the SPF to the maxillary line was 35.73 mm ± 2.47, and to the anterior head of the middle turbinate, it was 33.76 mm ± 4.52. Conversely, the average distance between the SPF and the basal lamella was found to be 9.71 mm ± 1.84. The mean distance to the choanal arch measured 8.78 mm ± 1.62, while the average distance from the SPF to the posterior fontanelle of the maxillary sinus ostium was 14.49 mm ± 1.32. Additionally, the distance between the SPF and the bony attachment of the inferior turbinate was 13.89 mm ± 2.01. The average height of the SPF above the nasal floor was recorded as 25.69 mm ± 2.43**.** Analysis of the data revealed no significant discrepancies in the measured distances when comparing the right and left sides of the nasal cavity (as shown in Table 1).

Table 1: Different measurements of the sphenopalatine foramen and its relations.

Cut of the CT scan	Distance	Side	Range(mm)	Mean± SD (mm)	T-test	P value
Axial	$SPFD_{AP}$ (mm)	Right	2.48 - 8.71	4.91 ±1.24		0.0030
		Left	2.53 - 8.94	4.9 ±1.25		
	SPF-ML (mm)	Right	27.44 - 46.49	35.65± 2.74	0.0915	0.0027
		Left	27.21- 45.10	35.56± 2.83		
	SPF-AH (mm)	Right	21.62- 49.13	33.59± 4.86	0.1024	0.0158
		Left	21.32- 49.08	33.43± 4.72		
	SPF-BL (mm)	Right	5.39- 13.27	8.98± 1.83	0.8949	0.0275
		Left	5.90- 13.64	9.43± 1.91		
	SPF-CA (mm)	Right	5.87- 13.19	8.73± 1.48	0.1359	0.0108
		Left	5.92- 12.90	8.92± 1.13		
	SPF-PF (mm)	Right	9.45-16.34	14.15± 1.13	0.0987	0.0091
		Left	9.43- 16.82	14.22±1.19		

Journal of Otorhinolaryngology and Facial Plastic Surgery 2023;9(1):1-9.
https://doi.org/10.22037/orlfps.v9i1.46872

Coronal	SPFD $_{cc}$ (mm)	Right	2.63 – 9.1	5.42 ±1.61	0.0396	0.0071
		Left	2.68 – 9.34	5.59 ±1.52		
	SPD-IT (mm)	Right	8.53-17.88	14.01±2.01	0.0031	0.0027
		Left	8.49-17.98	14.03±2.27		
	SPF-NF (mm)	Right	20.50- 30.58	25.78± 2.11	0.0097	0.0036
		Left	20.41- 30.79	25.81± 2.04		

SPFD$_{AP}$, anteroposterior diameter of the SPF; SPF-ML, distance between SPF and maxillary line; SPF-AH, distance between SPF and anterior head of the middle turbinate; SPF-BL distance between SPF and basal lamella; SPF-CA, distance between SPF and choanal arch; SPF-PF, distance between SPF and posterior fontanel ; SPFD$_{cc,}$, craniocaudal diameter of the SPF ; SPD-IT , distance between SPF and bony attachment of the inferior turbinate; SPF-NF, distance between SPF and nasal floor; SD: standard deviation, mm: millimeters, NS: non-significant.

Table 2: Various distances between SPF and different landmarks in different sexes.

Cut of the CT scan	Distance	Overall(mm)	Sex	Range (mm)	Mean± SD(mm)	T-test	P value
Axial	SPFDAP(mm)	5.01±1.37	Males	2.83 - 8.94	5.18 ±1.24	???	0.012
			Females	2.48 - 8.06	4.89 ±1.36		
	SPF-ML(mm)	35.73±2.47	Males	28.8 - 46.49	35.96 ± 2.90	2.9851	0.0057
			Females	27.21 -44.03	34.28 ± 2.33		
	SPF-AH(mm)	33.76±4.52	Males	21.89- 49.13	33.89± 4.96	0.265	0.0048
			Females	21.32- 48.92	33.43± 4.74		
	SPF-BL(mm)	9.71± 1.84	Males	5.87- 13.64	9.51± 1.84	0.1743	0.0180
			Females	5.39- 13.09	9.38± 1.79		
	SPF-CA(mm)	8.78± 1.62	Males	5.98- 13.19	8.99± 1.74	0.8770	0.0078
			Females	5.87- 12.41	8.27 ± 1.79		
	SPF-PF(mm)	14.49±1.32	Males	9.98- 16.82	14.87 ± 1.38	2.389	0.0024
			Females	9.73- 16.32	13.18 ± 1.49		
Coronal	SPFD cc(mm)	5.58 ±1.71	Males	2.98 - 9.34	5.79 ±1.84	0.7390	0.0193
			Females	2.63 - 8.99	5.10 ±1.38		
	SPD-IT(mm)	13.89±2.01	Males	9.02-17.98	14.12±1.98	0.8953	0.0028
			Females	8.49-16.53	13.62±1.82		
	SPF-NF(mm)	25.69±2.43	Males	20.41- 30.79	26.88± 2.41	3.989	0.0079
			Females	20.54- 26.95	24.27± 1.69		

SPFD$_{AP}$, anteroposterior diameter of the SPF; SPF-ML, distance between SPF and maxillary line; SPF-AH, distance between SPF and anterior head of the middle turbinate; SPF-BL distance between SPF and basal lamella; SPF-CA, distance between SPF and choanal arch; SPF-PF, distance between SPF and posterior fontanel ; SPFD$_{cc,}$, craniocaudal diameter of the SPF ; SPD-IT , distance between SPF and bony attachment of the inferior turbinate; SPF-NF, distance between SPF and nasal floor; SD: standard deviation, mm: millimeters, NS: non-significant

Discussion

Epistaxis, commonly encountered in clinical practice by otolaryngologists, remains one of the most frequent emergencies within the specialty. While many instances of epistaxis can be managed conservatively through interventions like nasal packing or the application of topical vasoconstrictors and cautery, certain cases—particularly those involving posterior epistaxis—are more challenging. Posterior epistaxis often arises from the sphenopalatine artery (SPA), necessitating surgical intervention, especially in recurrent or severe cases. The surgical ligation of the SPA has become the gold standard for managing such cases due to its high efficacy and relatively low risk of recurrence (7,8). The SPA, the terminal branch of the

Journal of Otorhinolaryngology and Facial Plastic Surgery 2023;9(1):1-9.
https://doi.org/10.22037/orlfps.v9i1.46872

maxillary artery, is a critical vessel supplying the nasal cavity, especially the posterior aspect. It originates within the pterygopalatine fossa and passes through the sphenopalatine foramen (SPF) into the lateral nasal wall. Given its role in posterior epistaxis, hemorrhage originating from the SPA can be particularly dangerous, sometimes leading to significant blood loss that necessitates urgent intervention. Endonasal endoscopic techniques have revolutionized the management of such cases, allowing for precise localization and ligation of the SPA with minimal invasiveness, a procedure that is life-saving in cases of uncontrolled bleeding (9).

SPA ligation is favored not only for its effectiveness, which has been reported to reach success rates as high as 89%. However, the end-artery nature of the SPA, limits collateral blood flow, thus reducing the risk of recurrence after ligation. In addition, studies have shown that SPA ligation is associated with reduced hospital stays and lower overall treatment costs when compared to more traditional methods like posterior nasal packing, which often requires extended observation while posing higher risks of complications such as, rebleeding and mucosal damage (8,10).

However, the success of SPA ligation can be significantly affected by anatomical variations in the SPF and the surrounding nasal structures. These variations exist in up to 10% of cases, potentially complicating the identification and ligation of the artery during surgery. Which are particularly challenging in patients who present with active bleeding secondary to anticoagulation therapy or after repeated attempts of nasal packing, as the mucosal and vascular structures become friable and difficult to distinguish. Therefore, a detailed understanding of the SPF's surgical anatomy, including knowledge of the different anatomical variations and spatial relationships with nearby structures, is crucial for the successful execution of SPA ligation (11).

Computed tomography (CT) has become an indispensable diagnostic tool, providing high-resolution images that are critical for preoperative planning in endoscopic sinus surgery (ESS) and other complex surgeries involving the nasal cavity, paranasal sinuses, skull base, and craniomaxillofacial regions. CT imaging enables visualization of detailed sinonasal anatomy, identification of anatomical variations, and more precise surgical approaches; thus reducing the risk of intraoperative complications. The ability of CT to offer detailed three-dimensional reconstructions makes it particularly valuable in navigating the complex anatomy of the nasal cavity and adjacent structures (12–14).

One of the major challenges in endoscopic sinus surgery is the accurate identification of the SPF, especially in the presence of anatomical variations or pathological changes such as polyps, tumors, or postoperative scarring. These variations can obscure the foramen, making it difficult to locate during surgery, especially when the patient presents with active epistaxis or is on anticoagulant therapy. The use of fixed bony landmarks visible on CT scans is therefore essential to ensure safe and effective localization of the SPF, which is crucial for the success of endoscopic procedures targeting the SPA (8,15). Despite the importance of accurate SPF identification, the literature on this topic is somewhat limited. Most studies have traditionally relied on cadaveric dissection to explore the anatomy of the SPF and its relationships with surrounding structures. However, cadaveric studies have inherent limitations, including tissue preservation artifacts that can distort the anatomy, thereby reducing the applicability of such findings to practical surgical events. This has led to a growing interest in CT-based studies, which offer more accurate and clinically relevant data on the anatomy of the SPF and its surrounding landmarks (16).

Nalavenkata et al. identified the posterior fontanel and the attachment of the inferior turbinate as reliable endoscopic landmarks for

Journal of Otorhinolaryngology and Facial Plastic Surgery 2023;9(1):1-9.
https://doi.org/10.22037/orlfps.v9i1.46872

accessing the SPF (17). These landmarks are particularly useful as they remain consistent even in the presence of variations in the surrounding anatomy. Then, Maxwell and colleagues expanded on this approach by proposing a set of five bony landmarks, easily identifiable on CT scans, that can guide surgeons to the most likely location of the SPF during endoscopic procedures. These landmarks include the maxillary line, the anterior head of the middle turbinate, and the basal lamella, among others, and are valuable because of their consistent presence across different patients, even after trauma or previous surgeries (8).

In the present study, we focused on several key anatomical landmarks, including the maxillary line, the anterior head of the middle turbinate, the basal lamella, the posterior fontanel, the choanal arch, the bony attachment of the inferior turbinate, and the nasal floor. These landmarks were chosen because they can be reliably identified through endoscopy, even in patients with a history of nasal surgery or trauma. Our findings show that the SPF is located, on average, 35.73 mm posterior to the maxillary line, 33.76 mm posterior to the anterior head of the middle turbinate, 9.71 mm from the basal lamella, and 14.49 mm posterior to the posterior fontanel. Additionally, the SPF is situated 8.78 mm anterior to the choanal arch, 13.89 mm above the bony attachment of the inferior turbinate, and 25.69 mm above the nasal floor. These measurements are consistent with the data reported in earlier studies, confirming the reliability of these landmarks for surgical navigation (18).

We observed that the distances between the SPF and the maxillary line, posterior fontanel, and nasal floor were significantly greater in males compared to females, reflecting the generally larger dimensions of the male nasal cavity. This finding aligns with the broader anatomical differences typically seen between sexes. However, no significant sex differences were noted in the distances from the SPF to the anterior head of the middle turbinate, basal lamella, choanal arch, or bony attachment of the inferior turbinate, suggesting that these landmarks can be reliably used in both sexes. Furthermore, the measurements were consistent between the right and left sides of the nasal cavity, indicating that these landmarks are symmetrical and can be used to guide bilateral procedures.

The dimensions of the SPF, measured in both the anteroposterior and craniocaudal planes, averaged 5.01 mm and 5.58 mm, respectively. These dimensions are consistent with previous findings by El-Shaarawy, further validating the use of these measurements in surgical planning (19).

In conclusion, we believe that the fixed bony landmarks identified in this study -which are easily visualized on CT scans of the paranasal sinuses- serve as valuable and reliable guides for rhinologists. By incorporating these landmarks into surgical practice, surgeons can reduce the time required for intraoperative localization of the SPA, thereby enhancing the precision and safety of procedures such as SPA ligation. This approach could complement traditional methods, such as reliance on the crista ethmoidalis, thus improving the overall surgical outcomes by minimizing the risk of complications and ensuring more consistent results across different patient populations.

Conclusion

Preoperative CT imaging plays a critical role in surgical planning by providing a clear and accessible view of several key bony landmarks within the nasal cavity. These landmarks are not only easy to identify but also serve as highly reliable reference points for the precise localization of the sphenopalatine foramen (SPF) during endoscopic procedures. In the context of posterior epistaxis, the ability to quickly and accurately identify these landmarks is particularly valuable. It allows surgeons to efficiently target and access the SPF, thereby streamlining the process of trans-nasal

Journal of Otorhinolaryngology and Facial Plastic Surgery 2023;9(1):1-9.
https://doi.org/10.22037/orlfps.v9i1.46872

endoscopic sphenopalatine artery ligation (TESPAL). By integrating these easily detectable anatomical markers into preoperative planning, surgeons can enhance the precision and speed of their interventions, making complex procedures like TESPAL more accessible and reduce the overall operative time.

Acknowledgments

Hearing Disorders Research Center, Loghman Hakim Hospital, Shahid Beheshti University of Medical Sciences, Tehran, Iran, financially supported this work.

Conflicts of Interest

The authors declare no conflicts of interest.

Financial Support

The authors declared that there was no external funding support for this study.

Ethics

IR.SBMU.RETECH.REC.1403.359

Authors ORCIDs

Afsoon Zandi
https://orcid.org/0009-0003-4492-3034
Ali Safavi Naini
https://orcid.org/0000-0001-5686-1094
Jahangir Ghorbani
https://orcid.org/0000-0001-6209-1081
Nasim Raad
https://orcid.org/0000-0003-1372-3710
Mahboobeh Karimi-Galougahi
https://orcid.org/0000-0001-9880-3802

References

1. Jeong H, Choi BY, Lee J, Kim KS, Min SJ, Kim JK. Prevalence and characteristics of S-point bleeding compared to non S-point bleeding in severe epistaxis. Braz J Otorhinolaryngol [Internet]. 2021;87(4):462–8. Available from: https://doi.org/10.1016/j.bjorl.2020.07.008

2. Hadoura L, Douglas C, McGarry GW, Young D. Mapping surgical coordinates of the sphenopalatine foramen: surgical navigation study. J Laryngol Otol. 2009;123(7):742–5. Available from: https://doi.org/10.1017/S0022215109004344

3. Douglas R, Wormald P-J. Update on epistaxis. Curr Opin Otolaryngol Head Neck Surg. 2007;15(3):180–3. Available from: DOI: 10.1097/MOO.0b013e32814b06ed

4. Elsheikh E, El-Anwar MW. Septal perforation and bilateral partial middle turbinate necrosis after bilateral sphenopalatine artery ligation. J Laryngol Otol. 2013;127(10):1025–7. Available from: https://doi.org/10.1017/S0022215113001904

5. Traboulsi H, Alam E, Hadi U. Changing trends in the management of epistaxis. Int J Otolaryngol. 2015;2015(1):263987. Available from: https://doi.org/10.1155/2015/263987

6. Seno S, Arikata M, Sakurai H, Owaki S, Fukui J, Suzuki M, et al. Endoscopic ligation of the sphenopalatine artery and the maxillary artery for the treatment of intractable posterior epistaxis. Am J Rhinol Allergy. 2009;23(2):197–9. Available from: https://doi.org/10.2500/ajra.2009.23.3294

7. Jeong H, Choi B, Lee J, Kim KS, Min SJ, Kim JK. Prevalência e características do sangramento no S-point em comparação com outros pontos sangramento na epistaxe grave. Braz J Otorhinolaryngol. 2021;87:462–8. Available from: https://doi.org/10.1016/j.bjorl.2020.07.008

8. Maxwell AK, Barham HP, Getz AE, Kingdom TT, Ramakrishnan VR. Landmarks for rapid localization of the sphenopalatine foramen: A radiographic morphometric analysis. Allergy Rhinol. 2017;8(2):ar-2017. Available from: https://doi.org/10.2500/ar.2017.8.0196

9. Prades JM, Asanau A, Timoshenko AP, Faye MB, Martin C. Surgical anatomy of the sphenopalatine foramen and its arterial content. Surg Radiol Anat. 2008;30:583–7. Available from: https://doi.org/10.1007/s00276-008-0390-x

10. Midilli R, Orhan M, Saylam CY, Akyildiz S, Gode S, Karci B. Anatomic variations of sphenopalatine artery and minimally invasive surgical cauterization procedure. Am J Rhinol Allergy. 2009;23(6):e38–41. Available from: https://doi.org/10.2500/ajra.2009.23.3403

11. Scanavine ABA, Navarro JAC, Megale SRM de CL, Anselmo-Lima WT. Estudo anatômico do forame esfenopalatino. Rev Bras Otorrinolaringol. 2009;75:37–41. Available from: https://doi.org/10.1590/S0034-72992009000100006

12. El-Anwar MW, Khazbak AO, Eldib DB, Algazzar HY. Lamina papyracea position in patients with nasal polypi: a computed tomography analysis. Auris Nasus Larynx. 2018;45(3):487–91. Available from: https://doi.org/10.1016/j.anl.2017.09.006

13. El-Anwar MW, Raafat A, Almolla RM, Alsowey AM, Elzayat S. Maxillary sinus ostium assessment: a CT study. Egypt J Radiol Nucl Med. 2018;49(4):1009–13. Available from: https://doi.org/10.1016/j.ejrnm.2018.07.009

Journal of Otorhinolaryngology and Facial Plastic Surgery 2023;9(1):1-9.
https://doi.org/10.22037/orlfps.v9i1.46872

14. El-Anwar MW, Ali AH, Almolla RM, Abdulmonaem G, Raafat A, Hassan ME. Radiological middle turbinate variations and their relation to nasal septum deviation in asymptomatic adult. Egypt J Radiol Nucl Med [Internet]. 2020;51(1):104. Available from: https://doi.org/10.1186/s43055-020-00222-1

15. Wareing MJ, Padgham ND. Osteologic classification of the sphenopalatine foramen. Laryngoscope. 1998;108(1):125–7. Available from: https://doi.org/10.1097/00005537-199801000-00024

16. Chiu T. A study of the maxillary and sphenopalatine arteries in the pterygopalatine fossa and at the sphenopalatine foramen. Rhinology. 2009;47(3):264. Available from: DOI: 10.4193/Rhin 08.153

17. Nalavenkata S, Meller C, Novakovic D, Forer M, Patel NP. Sphenopalatine foramen: endoscopic approach with bony landmarks. J Laryngol Otol. 2015;129(S3):S47–52. Available from: https://doi.org/10.1017/S0022215115000766

18. El-Anwar MW, Khazbak AO, Hussein A, Saber S, Bessar AA, Eldib DB. Sphenopalatine foramen computed tomography landmarks. J Craniofac Surg. 2020;31(1):210–3. Available from: https://doi.org/10.1097/scs.0000000000005857

19. El-Shaarawy EAA, Hassan SS. The sphenopalatine foramen in man: anatomical, radiological and endoscopic study. Folia Morphol (Warsz). 2018;77(2):345–55. Available from: https://doi.org/10.5603/FM.a2017.0104